EJN European Journal of Neuroscience

FENS Federation of European Neuroscience Societies

European Journal of Neuroscience, Vol. 39, pp. 1332–1342, 2013 doi:10.1111/ejn.12473

COGNITIVE NEUROSCIENCE

Functional connectivity-based parcellation of the human sensorimotor cortex

Xiangyu Long,[1] Dominique Goltz,[1,2] Daniel S. Margulies,[3,4] Till Nierhaus[1,4] and Arno Villringer[1,4]
[1]Department of Neurology, Max Planck Institute for Human Cognitive and Brain Sciences, Leipzig, Germany
[2]Institute of Psychology, University of Leipzig, Leipzig, Germany
[3]Max Planck Research Group: Neuroanatomy & Connectivity, Max Planck Institute for Human Cognitive and Brain Sciences, Leipzig, Germany
[4]Mind–Brain Institute at Berlin School of Mind and Brain, Charité-Universitätsmedizin Berlin and Humboldt University, Berlin, Germany

Keywords: post-task effect, resting-state functional magnetic resonance imaging, sensorimotor cortex, somatotopic, task-based

Abstract

Task-based functional magnetic resonance imaging (fMRI) has been successfully employed to obtain somatotopic maps of the human sensorimotor cortex. Here, we showed through direct comparison that a similar functional map can be obtained, independently of a task, by performing a connectivity-based parcellation of the sensorimotor cortex based on resting-state fMRI. Cortex corresponding to two adjacent Brodmann areas (BA 3 and BA 4) was selected as the sensorimotor area. Parcellation was obtained along a medial–lateral axis, which was confirmed to be somatotopic (corresponding roughly to an upper, middle and lower limb, respectively) by comparing it with maps obtained using motoric task-based fMRI in the same participants. Interestingly, the resting-state parcellation map demonstrated higher correspondence to the task-based divisions after individuals performed the motor task. Using the resting-state fMRI data, we also observed higher functional correlations between the centrally located hand region and the other two regions, than between the foot and tongue. The functional relevance of these somatosensory parcellation results indicates the feasibility of a wide range of potential applications to brain mapping.

Introduction

Classical approaches for parcellating the cerebral cortex are based on histological features (Brodmann, 1909; Vogt & Vogt, 1919; Economo, 1926; Sanides, 1970; Triarhou, 2007). The high interindividual variability of the anatomical/functional areas and the difficulty of using non-invasive imaging techniques to identify histological features of brain tissue are the main motivations for developing novel parcellation approaches (Amunts *et al.*, 1999; Geyer *et al.*, 2011; Van Essen & Glasser, 2013). With non-invasive functional magnetic resonance imaging (fMRI), the cerebral cortex can be parcellated into different functional units via motivated tasks (Heeger & Ress, 2002). Recently, several groups have developed task-free methods based on measures of structural and functional connectivity for the parcellation of the human cerebral cortex, e.g. Broca area (Anwander *et al.*, 2007; Kelly *et al.*, 2010), lateral premotor cortex (Schubotz *et al.*, 2010), temporal pole (Fan *et al.*, 2013), thalamus (Serra *et al.*, 2013), cingulate cortex (Beckmann *et al.*, 2009; Yu *et al.*, 2011), primary motor (MI) area (Gorbach *et al.*, 2011; Nebel *et al.*, 2012), medial frontal cortex (Johansen-Berg *et al.*, 2004), frontal pole (Liu *et al.*, 2013), lateral frontal cortex (Goulas *et al.*, 2012), inferior parietal cortex (Ruschel *et al.*, 2013), precuneal cortex (Margulies *et al.*, 2009; Zhang & Li, 2012), lateral parietal cortex (Nelson *et al.*, 2010), anterior cingulate cortex (Margulies *et al.*, 2007) supplementary motor area (Kim *et al.*, 2010) and primary somatosensory (SI) cortex (Roca *et al.*, 2010), etc. The advantage of these methods is that no modality-specific tasks are necessary to identify functional subregions, making it an ideal approach for characterising brain organisation in clinical and longitudinal studies (Knosche & Tittgemeyer, 2011; de Reus & van den Heuvel, 2013; Wig *et al.*, 2013b).

We aimed to parcellate the human sensorimotor cortex, consisting of the contiguous MI and SI areas, into functionally meaningful subunits using resting-state fMRI (rs-fMRI) data. Based on their cytoarchitecture, the MI includes Brodmann area (BA) 4 (Campbell, 1905), and the SI includes BA 3, BA 1 and BA 2 (Brodmann, 1909; Vogt & Vogt, 1919; Geyer *et al.*, 1999, 2000). The sensorimotor cortex presented somatotopic organisation, with subregions relating to different body parts (Penfield & Boldrey, 1937; Kaas *et al.*, 1979; Okada *et al.*, 1984). This organisation within the SI/MI was also found via multiple motor/tactile tasks (Rao *et al.*, 1995; Stippich *et al.*, 1999; Lotze *et al.*, 2000; Meier *et al.*, 2008; Buckner *et al.*, 2011).

Recently, the subregions within the sensorimotor cortex were found to be organised ventral-to-lateral using rs-fMRI or diffusion-weighted imaging (van den Heuvel & Hulshoff Pol, 2010; Roca

Correspondence: Daniel Margulies, [3]Max Planck Research Group: Neuroanatomy & Connectivity, as above.
E-mail: margulies@cbs.mpg.de

Received 26 November 2013, accepted 5 December 2013

et al., 2010; Cauda *et al.*, 2011; Yeo *et al.*, 2011; Jo *et al.*, 2012; Nebel *et al.*, 2012). Whether the extent of parcellations based on rs-fMRI data spatially corresponds to these somatotopic subdivisions remains to be quantitatively assessed. In the present study, we assessed whether the parcellation of the primary sensorimotor cortex using rs-fMRI corresponds to the representations of upper–middle–lower limb segmentation.

Materials and methods

Data

Two datasets were included in the present study (Dataset I and II). Each dataset was composed of rs-fMRI and motor task fMRI data for the aim of comparing the results of functional connectivity-based parcellation with the task-induced activation related to the movement of body parts. Dataset I included one resting-state session that was scanned after a task session in order to investigate the post-task effect on the parcellation analysis.

Dataset I: Max Planck Institute

Participants

Nine right-handed adult participants were enrolled in the present study at the Max Planck Institute (MPI) for Human Cognitive and Brain Sciences in Leipzig (two females; age 27 ± 2.12 years). All participants were enrolled from the local university and had no history of any psychiatric or neurological disease. The present study was approved by the local ethics committee and written informed consent was given by each participant. The Code of Ethics of the World Medical Association (Declaration of Helsinki), printed in the *British Medical Journal* (18 July 1964), was followed by the present study.

Magnetic resonance imaging data acquisition

All data were acquired using a 3-Tesla magnetic resonance imaging system (Verio, Siemens, Erlangen, Germany) equipped with a 32-channel head-coil. The common parameters for all fMRI sessions were as follows: gradient-echo echo-planar imaging sequence, interleaved slice-timing, gap, 1 mm; repetition time (TR), 2 s; echo time (TE), 30 ms; flip angle, 90º; matrix size, 64 × 64. For each participant, five fMRI sessions were acquired with a break of 10 s in between (Fig. 1C). The first two sessions and the fourth session were resting-state sessions of 6 min each. The third and fifth sessions were motor-task sessions of 12 min each. For the resting-state sessions, 30 axially-oriented slices over the whole brain were collected with a voxel size of 3 × 3 × 4.8 mm. For the task sessions, 20 coronally-oriented slices with a voxel size of 2 × 2 × 2.2 mm were obtained surrounding the central sulcus (Fig. 1A). The parameters for the magnetization-prepared rapid gradient-echo (MPRAGE) T1-weighted image sequence were: 12-channel coil, flip angle, 9°; 176 slices; TR, 2300 ms; TE, 2.96 ms; voxel size, 1 × 1 × 1 mm; matrix size, 240 × 256; inversion time, 900 ms. Visual projection was by a mirror fixed to the head-coil and a projector located outside the scanner room.

Participants lay supine in the scanner with their head fixed using foam pads to minimise head motion. During the three resting-state sessions (i.e. Rest1, Rest2 and Rest3), participants were instructed to focus on a white fixation cross with a black background, and to remain motionless and not think of anything in particular. Rest3 was scanned after the first task session for the post-task effect investigation.

During the task session (i.e. Task1 and Task2), participants were asked to perform a movement task (Fig. 1B). Each block included 25 s of active movement and 15 s of rest. There were three types of movements in this task: 'tapping right fingers', 'moving tongue within the mouth', and 'moving right foot and toes'. All movements were performed at a self-defined pace throughout the active block. The German word for the respective body part ('Hand', 'Fuß' or 'Zunge') was displayed in place of the cross to indicate which body part to move. The word was projected in white with a black background in the center of the mirror. For each body part, six blocks were counterbalanced.

Dataset II: Human Connectome Project

A second dataset was provided by the Human Connectome Project (HCP), supported by the WU–Minn Consortium and McDonnell Center for Systems Neuroscience at Washington University (Van Essen *et al.*, 2013). The dataset consisted of 68 left-handed and right-handed healthy participants (50 females) in the HCP quarter 1 (released online: March 2013). Thirty-six participants (18 females, age 26–35 years) were selected for the present study, with specific attention paid to matching male and female participants.

For each participant, one rs-fMRI session (with left-to-right direction phase encoding) and the motor task fMRI session were analysed. The scan parameters of the rs-fMRI data were: TR, 720 ms; TE, 33.1 ms; flip angle, 52°; field of view,

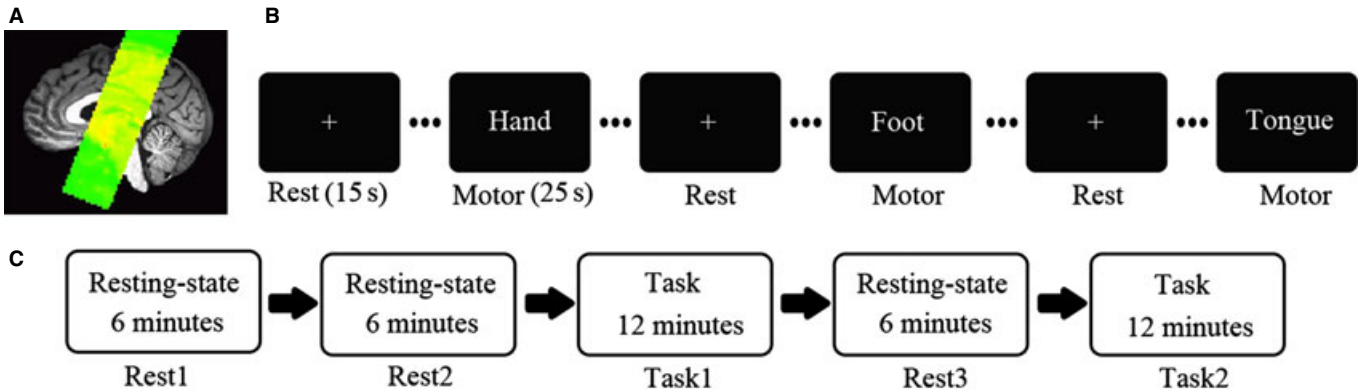

FIG. 1. Both resting-state and task-based data were included in the present study. (A) The green area represents the slices obtained during the task session for each participant. (B) A block-design paradigm was used in the task session. Visual stimuli instructed participants to move the respective body parts. (C) The experiment consisted of five sessions including resting periods and tasks, and lasted for approximately 1 h. The gap between sessions was around 20 s.

208 × 180 mm; slice thickness, 2.0 mm; 72 slices; voxels isotropic, 2.0 mm; multiband factor, 8; echo spacing, 0.58 ms; Bandwidth (BW), 2290 Hz/Px; time points, 1200 (Feinberg *et al.*, 2010; Moeller *et al.*, 2010; Setsompop *et al.*, 2012; Xu *et al.*, 2012). The task paradigm was similar to that used in the acquisition of the MPI dataset. Participants were asked to move their right or left hand, toes and tongue with 12-s blocks and a 3-s cue. A total of 284 time points were obtained during the motor task session.

Analysis

Dataset I: Max Planck Institute

All images were preprocessed as follows using SPM5 (www.fil.ion.ucl.ac.uk/spm/): slice-timing correction, motion correction, spatial normalisation to the Montreal Neurological Institute 152 space, sampled to 3 × 3×3 mm voxel size, and spatial smoothing with 6-mm full-width at half-maximum of the Gaussian kernel. All participants had < 1 voxel translation (3 mm) or 1° rotation head motion. For the resting-state data, the REST toolbox (www.restfmri.net/) was used with the following parameters: (i) band-pass filtering (0.01–0.08 Hz); (ii) removing the linear trend of time courses; and (iii) regressing out six head motion parameters, average time courses from a white matter mask and a cerebral spinal fluid mask (Fig. 2).

Task-based analysis

The activation maps of each body part were generated using a general linear model analysis in SPM5. A one-sample *t*-test was performed on the beta intensity maps across participants for each body part. All t-maps were thresholded at $p < 0.05$ using AlphaSim in AFNI (Cox, 1996).

Connectivity-based parcellation analysis

The connectivity-based parcellation analysis was the same for all three resting-state sessions (see Fig. 2).

1 Considering the anatomical variations across participants and the spatial resolution of fMRI data, we selected an area including both the MI and SI along the central sulcus. A template mask including the left BA 4 and BA 3 from the Anatomy toolbox was selected as the region of interest (ROI; Fig. 2-1; Geyer *et al.*, 1999, 2000; Eickhoff *et al.*, 2005).

2 Spatial correlation maps between each voxel within the ROI were calculated and transformed using Fisher's r-to-z (Vincent *et al.*, 2007; Yeo *et al.*, 2011; Fig. 2-2).

3 An eta^2 value was then calculated for each pair of voxels' z-transformed connectivity maps, generating a similarity matrix (Fig. 2–3) for each individual (Cohen *et al.*, 2008). Group-level analysis was conducted on data averaged across each resting-state session from each participant separately.

4 Finally, both the individual similarity matrix and group-averaged matrix were classified into between two and 10 clusters by spectral K-means using the multicut clustering algorithm (Fig. 2-4/5; with 1000 iterations using the Spectral Clustering Toolbox; Meila & Shi, 2001; Kelly *et al.*, 2010).

5 The optimal number of clusters was investigated using two approaches at the group level. The Dice coefficient (DC; from 0 to 1, where 1 is the highest overlap) was calculated for each *k*'s

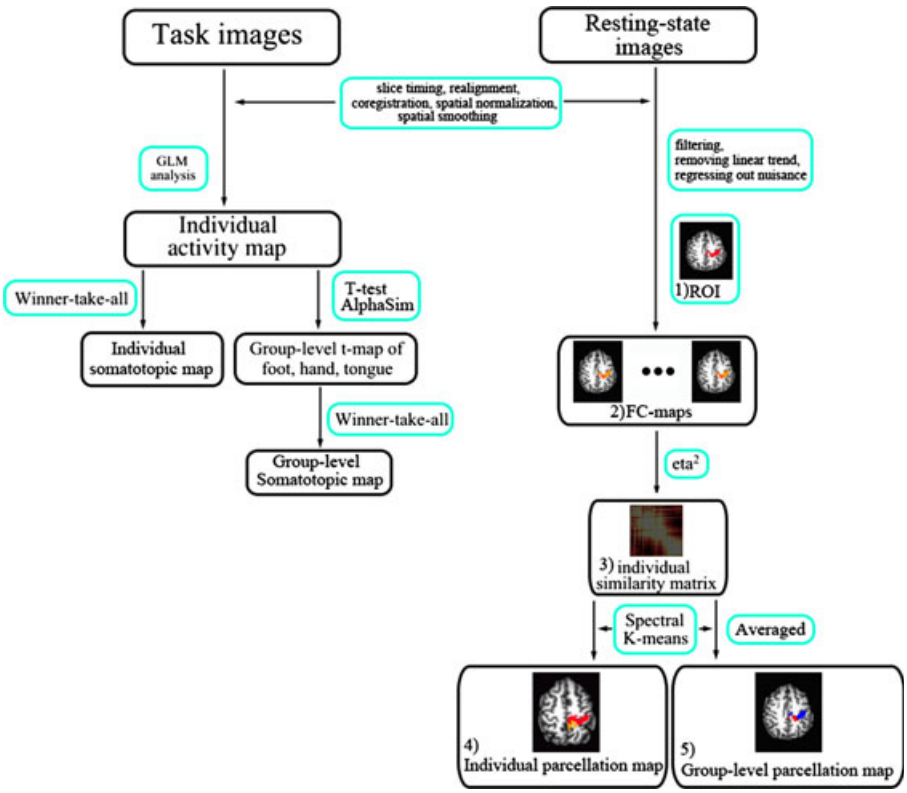

FIG. 2. The processing steps for task and resting-state data. 5 steps are displayed for the parcellation analysis: 1) The ROI selection; 2) The functional connectivity analysis; 3) Generating the similarity matrix; 4) and 5) Generating the parcellation maps. The black frame indicates the results, and the blue frame indicates the processing methods. The task images provided activation areas for foot, hand and tongue. From the resting-state images, clusters were generated based on the correlation maps of voxels within the ROI. The results of the task and resting-state sessions were further analysed for similarity using the DC. FC, functional connectivity; GLM, general linear model.

solution between the first and second resting-state sessions to test the stability of each k (Dice, 1945; Nebel *et al.*, 2012). In addition to the DC calculation, the silhouette was also calculated for the three MPI resting-state sessions (Kelly *et al.*, 2010). The silhouette value is a ratio between the similarity of a voxel to others within the same cluster and to those outside it. A higher silhouette indicated higher reliability of the clusters.

Assessment of correspondence between task and resting state

Three assessments evaluated the spatial correspondence between task-derived regions and the resting-state clusters.

Group-level analysis

A winner-take-all (WTA) analysis was performed on the group-level t-maps of two task sessions derived from the foot, hand and tongue within the left BA 3 and BA 4 ROI (Meier *et al.*, 2008). A voxel was assigned as one limb area if the t-value of one body part was higher than the others. The overlap ratio was then calculated between the WTA map and the three-cluster parcellation map from three resting-state sessions. The DC was also calculated between WTA maps of the two task sessions. Here the overlap ratio between two maps that both had three clusters was not calculated cluster by cluster as the normal DC. As both maps had the same number of clusters and the same ROI size, the overlap ratio was calculated by summing the number of overlap voxels for each pair of clusters, and then dividing it by the number of voxels within the whole ROI.

Individual-level analysis

WTA analysis was performed on each individual's Task1 t-maps of the foot, hand and tongue within the ROI. For each k solution, the DC was calculated between the area of the WTA map and the clusters from the Rest1 parcellation map. The three highest cluster pairs were averaged. The parcellation map with the highest average DC is presented (Fig. 5). In addition, the averaged maximum DC value between the Task1 WTA maps and the parcellation map of the Rest2 and Rest3 was also calculated for each participant.

Within each cluster of the resting-state parcellation map ($k = 3$ for each session), the averaged and SD values of Task1's group-level t-maps (foot, hand and tongue) were calculated.

Assessing relationships between body parts

For the MPI data, a 6-mm radius sphere was created for the representations of each body part centered on the group-level peak voxel from each (foot: [−3, −24, 75]; hand: [−39, −21, 60]; tongue: [−54, −9, 33], MNI standard space). For each participant, the average time series within each sphere were correlated from the three resting-state sessions.

Three clusters, which were selected from the parcellation maps of each resting-state session, were used as the upper, middle and lower limb regions. The correlation coefficients between these clusters were then calculated (in Fig. 3B: red cluster, lower limb region; green cluster, middle limb region; yellow cluster, upper limb region). For both correlation coefficients (one obtained from Task1 and the other from resting-state clusters), a paired t-test between middle–lower (i.e. hand–foot), lower–upper (i.e. foot–tongue) and middle–upper (i.e. hand–tongue) was performed across participants.

Dataset II: Human Connectome Project

All fMRI data were first preprocessed in the HCP pipeline using FSL (FMRIB Software Library, Woolrich *et al.*, 2001; Jenkinson *et al.*, 2002, 2012; Fischl, 2012; Glasser *et al.*, 2013). For the resting-state data, the REST toolbox was used as described for the MPI dataset: band-pass filtering, removing linear trend of time courses, regressing out six head motion parameters, average time courses from a white matter mask and cerebral spinal fluid mask. For the task data, only the activation of the right hand, right foot and tongue were selected. The WTA map was created based on the t-map of these three body parts.

The parcellation analysis for the HCP quarter 1 data was performed in the same way as for the MPI data. The BA 3/4 ROI was used. The similarity matrix for each participant was generated via the connectivity-based analysis. Three clusters were detected on the group-level averaged similarity matrix using the spectral K-means approach. The DC between the WTA map and group-level parcellation map was calculated.

Results

Activation areas for body parts

The general linear model analysis of the task sessions revealed activation areas for the hand, foot and tongue for both task sessions. Here we only focus on activations within the SI and MI. Owing to the sensory aspect implicit in any motor task, the SI and MI were both activated. The foot region was detected in the left paracentral lobule, the hand region in the left pre/postcentral gyrus, and the tongue region in the bilateral inferior post/precentral gyrus (Fig. 3A). The activation areas for all body parts were consistent across both task sessions. In addition, the upper–middle–lower limb segmentation was represented in the WTA map (Fig. 3B). The DC between two WTA maps of two task sessions was 0.9516.

Clustering of resting-state data

Three subregions were found on the group-level connectivity-based parcellation analysis using the resting-state data (Fig. 3B, second row). Consistent with hypotheses of somatotopic organisation, the superior-most region was located ventromedially, a second region was located dorsolaterally and a third region was located inferiolaterally. This spatial distribution was similar across three resting-state sessions. This somatotopic organisation was also found in the parcellation maps with different cluster numbers (Fig. 3C).

The Dice coefficients (DCs) between the parcellation maps of the two resting-state sessions indicated that high stability was found when k was 3 (Fig. 4A). Across the three resting-state sessions, the silhouette value was the highest when k was 2, and the second highest value in k was 3. All silhouette values did not change dramatically across all k solutions (Fig. 4B).

Correspondence between task regions and resting-state subregions

At the group-level, resting-state subregions corresponded to the subregions observed in the task-based WTA map. All three parcellation maps demonstrated a high DC (> 0.75) with the task's WTA map (Fig. 3B). Individual DCs between the parcellation map from the Rest1 and the WTA map from Task1 are shown in Fig. 5A. All

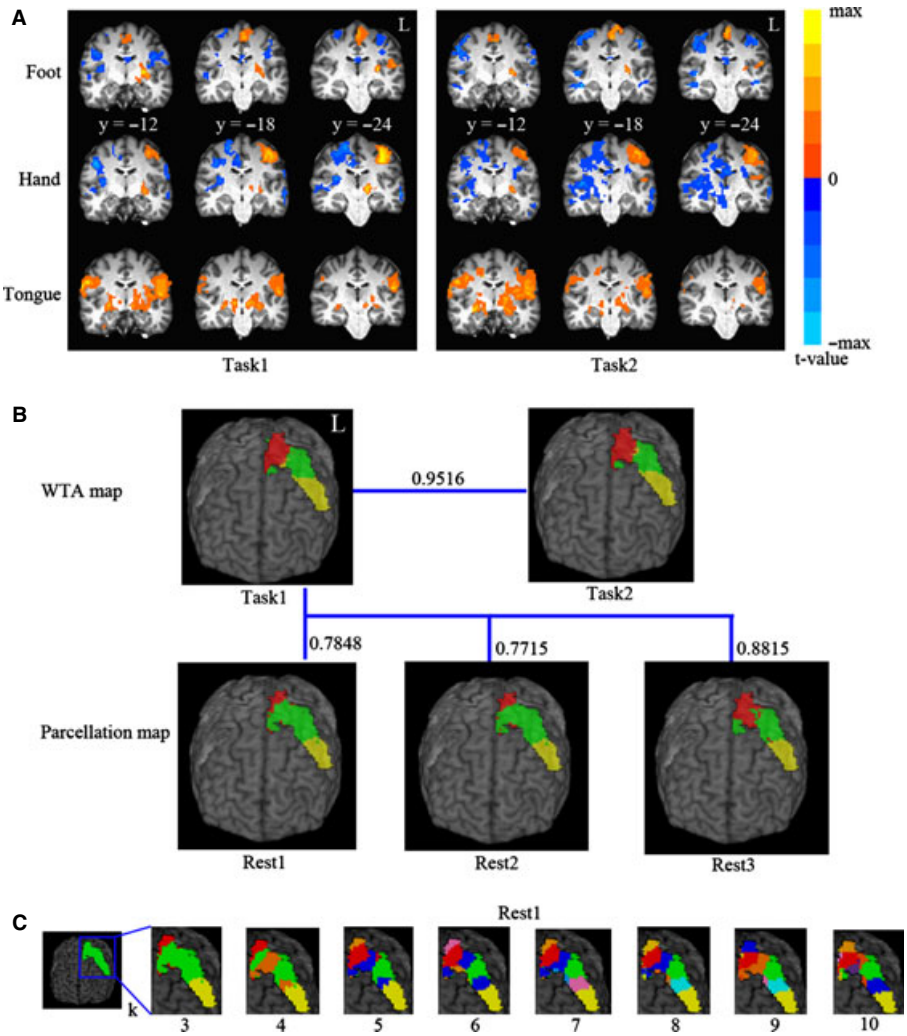

FIG. 3. (A) Each row represents the result from one body part. The group-level activity regions of right foot, right hand and tongue were found in both task sessions. All t-maps were corrected at $P < 0.05$ and merged on one participant's structural T1 image. Warm color represents positive value and cold color represents negative value. The coordinates are in Montreal Neurological Institute space. L, left hemisphere. (B) The upper row shows the group-level WTA map across three t-maps of right foot, right hand and tongue from the two task sessions. Yellow color represents upper limb, green color represents middle limb and red color represents lower limb. The lower row presents the map from the group-level functional connectivity-based parcellation analysis of three resting-state sessions. Number of clusters (k) was set to three. The colors corresponding to three clusters are yellow, green and red. The DC between each pair of maps is presented near the blue lines. (C) The parcellation maps from Rest1 with different numbers of clusters are presented. Different colors indicate different clusters.

participants' maximum overlap DC ratios were greater than 0.55. The highest DC in several individuals was observed for $k > 3$ due to the detection of small clusters (e.g. s04 and s07) in the parcellation analysis.

The averaged and SD values of three t-maps of Task1 within each cluster are presented in Fig. 6. Each cluster from resting-state data had the highest value to the t-map from only one body part. Their spatial distribution was also somatotopically organised.

Post-task effect on the parcellation analysis

At the group level, the parcellation map of Rest3 presented the highest DC with Task1's WTA map (Fig. 3B). At the individual level, an increased trend of DC was observed from Rest1/Rest2 to Rest3 (Fig. 5B). Rest3 presented a significantly higher DC than Rest2 and Rest1 ($P < 0.05$) across participants. No significant difference was found between Rest1 and Rest2 (Fig. 5B).

Relationships between three body parts

The hand–foot, hand–tongue and foot–tongue correlation, using the task-peak sphere and the clusters from the parcellation analysis, were also examined across three resting-state sessions (Table 1, left). Both the hand–foot and hand–tongue correlation were significantly higher than the foot–tongue correlation across participants and the first two resting-state sessions. Moreover, there was no significant difference between the hand–foot and hand–tongue correlation (Table 1, right).

Results from the Human Connectome Project data

The activity areas of the right foot, right hand and tongue were similar to those found in the MPI dataset (Fig. 7A), and the somatotopic organisation was also observed. High correspondence between the task WTA map and resting-state parcellation map was detected (Fig. 7B; DC = 0.8441).

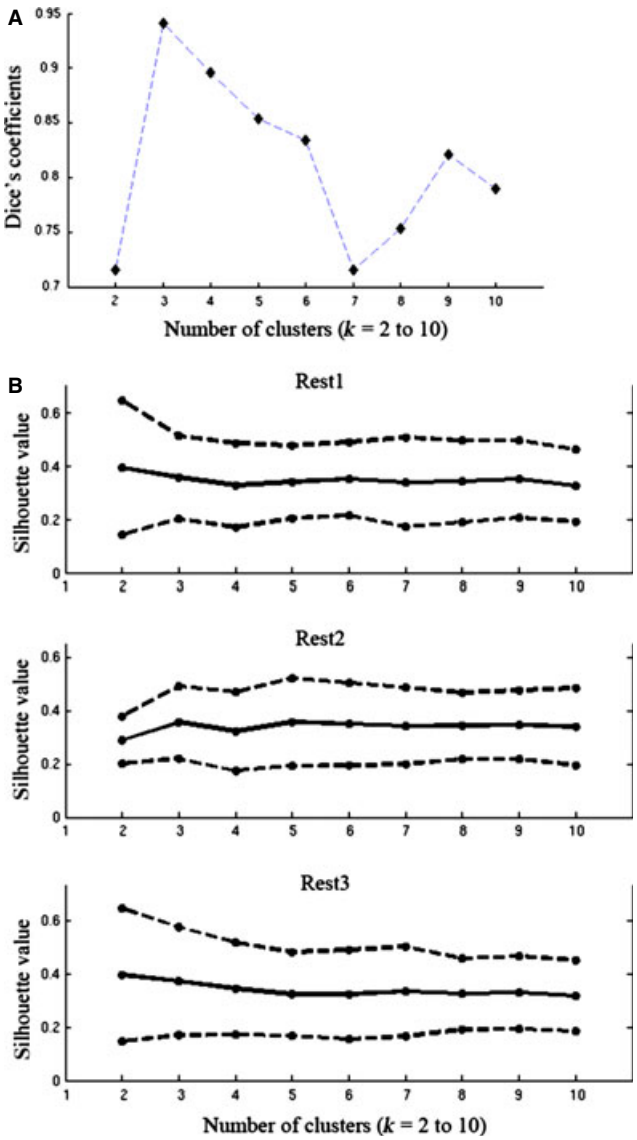

FIG. 4. (A) The DC value between the parcellation maps of Rest1 and Rest2 across different *k*. Each diamond shape represents one selection of *k* for the DC calculation between two close resting-state sessions' parcellation maps. (B) The silhouette value of the detected clusters across three resting-state sessions. The mean and SD value are presented. The solid line indicates the mean value, and the dashed line indicates the SD.

Discussion

We observed that rs-fMRI-based parcellation of the sensorimotor cortex, corresponding to BA 3 and BA 4, identifies somatotopically arranged clusters in two independent datasets. These clusters correspond spatially to a somatotopic representation of upper–middle–lower limb segmentation, as identified by task-based fMRI. Interestingly, the resting-state parcellation map demonstrated higher correspondence to the task-based divisions after individuals performed a motor task.

Somatotopic organisation revealed by resting-state functional magnetic resonance imaging

We found somatotopic organisation within the left sensorimotor cortex. Precentral and postcentral gyrus (motor and somatosensory) regions were subdivided into three clusters, depending on the individual dataset, from dorsomedial to ventrolateral along the central gyrus (Fig. 3). Considering the spatial resolution of fMRI and the variation of anatomical structure near the central sulcus across participants, we applied the connectivity-based parcellation analysis on the conjunction of the MI and SI. Before the present study, several previous studies had also found similar distribution of clusters within the MI and SI by connectivity-based parcellation analysis (Roca *et al.*, 2010; Schubotz *et al.*, 2010; Gorbach *et al.*, 2011; Nebel *et al.*, 2012). Although the number of clusters was variable, dorsomedial–ventrolateral organisation was a common feature across these studies. The whole-brain voxel-wise connectivity-based parcellation analysis also detected two parts of the somatomotor area, dividing it into a lower face and upper hand–foot region during rest (Yeo *et al.*, 2011). Our study confirmed that this somatotopic organisation could be found using rs-fMRI data, and this organisation was reliable across different resting-state sessions and datasets. Importantly, we validated the somatotopic arrangement by showing the correlation between subregions identified by resting-state-based parcellation and representations of body parts as identified by task-based fMRI. Different body sectors seem to have characteristic functional connectivity features along the central gyrus that have separable domains (van den Heuvel & Hulshoff Pol, 2010).

Resting-state clusters and activations related to different body parts

We compared resting-state clusters and activation areas from the task (Figs 3 and 6). For both datasets, firstly, three clusters were found in the group-level analysis. These clusters were equally distributed and displayed high correspondence with the WTA map derived from the tasks (Figs 3 and 6). A high overlap (DC > 0.75 for the MPI dataset; DC = 0.8441 for the HCP quarter 1 dataset) confirmed three distinguishable areas using two different fMRI modalities. Similar results were also found at the individual level (Fig. 4A). The averaged value within each resting-state cluster showed a good one-to-one correlation with the respective cerebral representations of the different body parts (Fig. 5). Previous studies had reported that the motor cortex consists of three separate sectors: lower body, middle section and head (Meier *et al.*, 2008; Yeo *et al.*, 2011; Weiss *et al.*, 2012). According to our approach, these three sectors could be distinguished from the others based only on the resting-state functional connectivity patterns within the sensorimotor cortex.

The post-task effect to the parcellation analysis

The Rest3 session was scanned after the Task1 session. Interestingly, the parcellation maps of Rest3 showed higher correspondence with the Task1 WTA map than the other two resting-state sessions at both the group- and individual-level. It was reported that the resting-state needs a period of time to return to a task-free baseline state after the performance of tasks (Barnes *et al.*, 2009), and motor learning can affect subsequent activity within resting-state networks (Albert *et al.*, 2009). The repetitive movements of alternate body parts could be considered as a simple training task, and this task affected the sensorimotor cortex functional organisation in the following resting state as the gap between Task1 and Rest3 was short (around 20 s). The subdivisions of the sensorimotor cortex might consolidate and vary through motor-training tasks (Taubert *et al.*, 2011; Tung *et al.*, 2013). It was also possible that participants

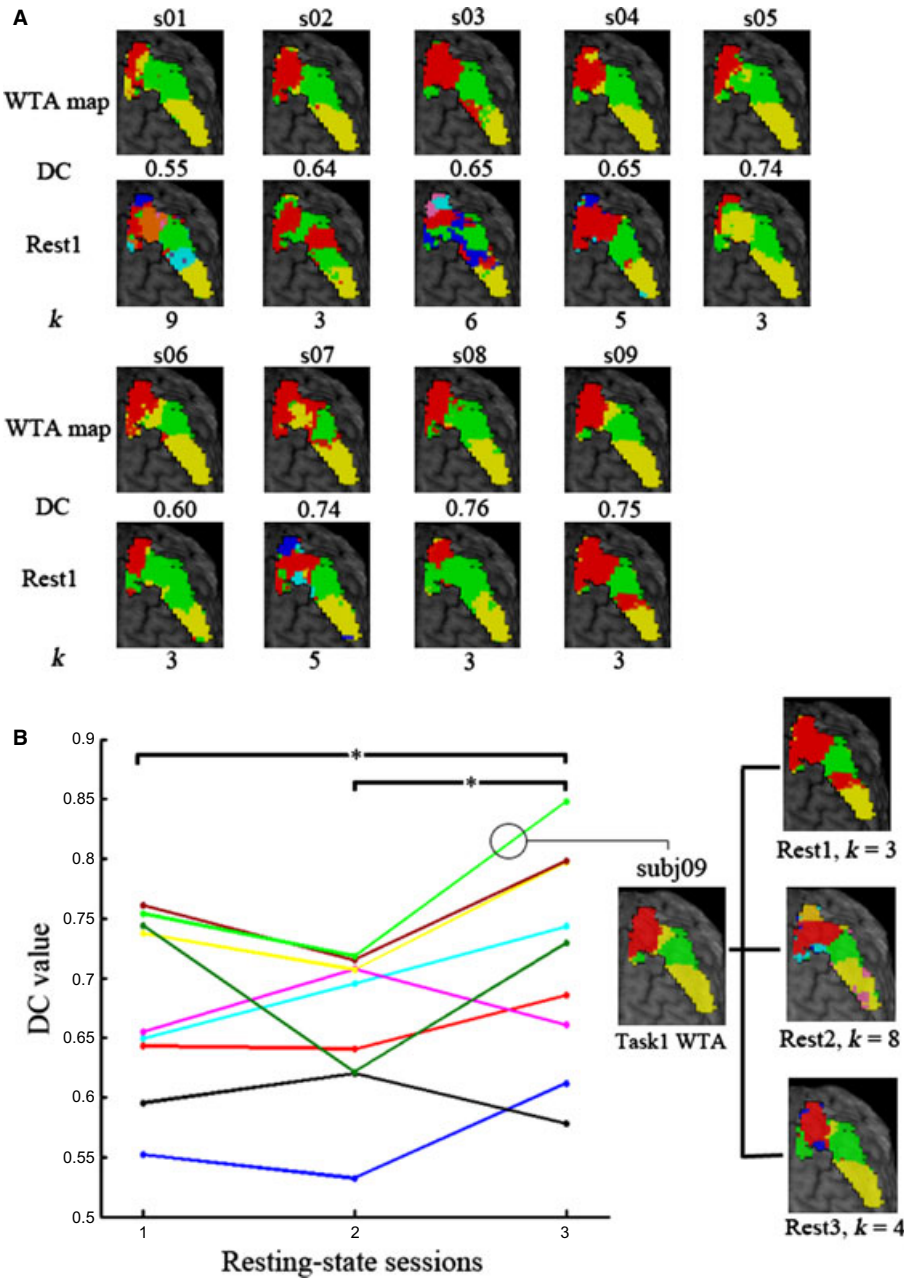

FIG. 5. (A) The parcellation map that gives the highest averaged DC and the WTA map for each participant are displayed. The DC is presented between these two maps. The *k*-solution that had the maximum averaged DC for each participant is indicated below. (B) The averaged maximum DC values between the Task1 WTA maps and resting-state parcellation maps are presented for each participant across three resting-state sessions. One color indicates one participant. The dots represent the averaged maximum DC value for each resting-state session. *Significant difference between sessions ($P < 0.05$). One participant's WTA map of Task1 and parcellation maps of three resting-state sessions are displayed (i.e. green line in B).

imagined the previous motor tasks during the resting session, thereby activating it (Stippich *et al.*, 2002). Duff *et al.* (2008) found that the task-activated regions presented increased signal spectral power in the post-task session. To our knowledge, this is the first time that this plasticity effect was detected in the resting-state functional connectivity-based parcellation analysis. We suggested that the functional subregions that were detected during the resting state should take task effects into account. This effect could also lead the morphometry difference between task-based regions and resting-state regions.

Robust activations corresponding to body parts by movement task

For the MPI dataset, each participant performed three different movements engaging the foot, hand, and tongue. The motoric activity was inherently accompanied by sensory stimulation. We asked participants to perform these tasks in two separate sessions, in order to identify whether the activations were robust and consistent. Several studies had previously reported somatotopically arranged functional regions corresponding to the hand, foot and tongue within the

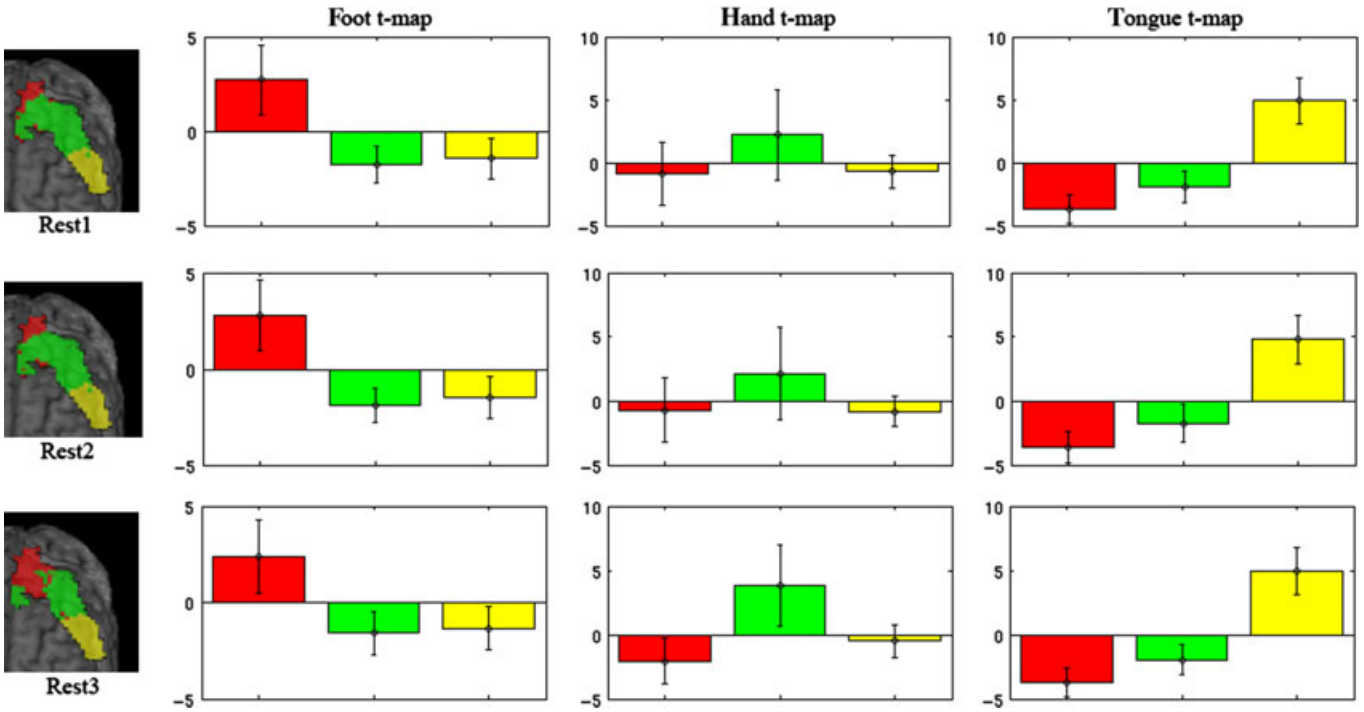

FIG. 6. For each row, the three-cluster parcellation map from the resting-state session was merged on one participant's T1 image. Each color represents one cluster. The averaged and confidence intervals of *t*-values from the Task1 t-map of the right foot, right hand and tongue within each cluster are given, respectively. The color of each bar picture was assigned according to each cluster.

TABLE 1. Correlation analysis of body part ROIs

Session	*r* (rest)	*r* (task)		Rest ROI	Task ROI
Rest1					
Hand–foot	0.8986	0.5321	H–F > F–T	0.0001	0.0227
Hand–tongue	0.8316	0.5096	H–T > F–T	0.0062	0.0324
Foot–tongue	0.5317	0.2292	H–F > H–T	0.5890	0.8538
Rest2					
Hand–foot	0.8016	0.5700	H–F > F–T	0.0005	0.0114
Hand–tongue	0.9493	0.6744	H–T > F–T	0.0078	0.0027
Foot–tongue	0.5427	0.3365	H–F > H–T	0.3088	0.3481
Rest3					
Hand–foot	0.9820	0.4544	H–F > F–T	0.0004	0.0096
Hand–tongue	0.7794	0.6503	H–T > F–T	0.1347	0.0110
Foot–tongue	0.6434	0.2221	H–F > H–T	0.0209	0.1559

H, hand; F, foot; T, tongue.

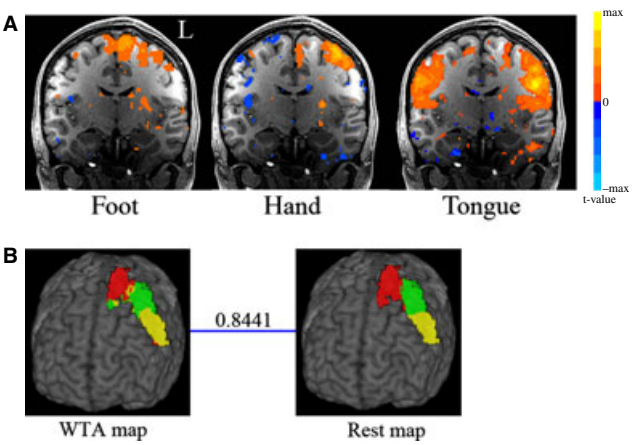

FIG. 7. (A) The group-level activity maps of the right foot, right hand and tongue are displayed. Coordinate Y is 12 mm in Montreal Neurological Institute space. Warm color represents activation and cold color represents deactivation. L, left. (B) The WTA map and parcellation map are presented. The DC between these two maps is above the blue line. For the WTA map, the upper, middle and lower limb area was indicated in yellow, green and red. The red, green and yellow color in the parcellation map indicates clusters.

MI and SI using task-based fMRI (Meier *et al.*, 2008; Buckner *et al.*, 2011; Weiss *et al.*, 2012), and the results have been shown to be highly reproducible across different sessions (Weiss *et al.*, 2012). Our results showed similar stability of upper–middle–lower limb segmentations across the two task sessions (Fig. 3). These patterns were also found in the HCP quarter 1 dataset (Fig. 7A). These results provide initial validation for describing the somatotopic arrangement of subareas derived exclusively from rs-fMRI data.

Relationships between representations of body parts

The rs-fMRI data also allowed us to investigate the correlations between the different somatotopically arranged clusters. The ipsilateral right foot–hand and hand–tongue show similar correlation values, which were both higher than the foot–tongue relationship. The foot–tongue presented no significant correlation. This result was similar to the findings of Yeo *et al.* (2011). They found a higher correlation between the right foot–hand than between hand–tongue, and the lowest correlation between foot–tongue. Unlike the current findings, Yeo *et al.* (2011) found the foot–tongue to have a significant correlation. Although these different results may be explained by the substantially larger sample size (n = 1000) in the study of Yeo *et al.* (2011), the ranking of the three pairs was nonetheless consistent.

Although the spatial proximity of hand, foot, and tongue representation in the brain may contribute to the current findings, the

correlation of the blood oxygenation level dependent (BOLD) signal between body parts may also be explained by basic motor habits. The hands and feet present high interlimb coordination (Swinnen & Carson, 2002), and hand and tongue coordination is frequently necessary, e.g. during talking and eating (Gentilucci & Campione, 2011). In contrast, the foot and tongue are rarely behaviorally coupled. Spontaneous movements (or movement inhibition) in the magnetic resonance imaging scanner could also contribute to our findings.

Limitations

Although a 'standard' spatial resolution of 3 mm^3 was used in the present study, it might not be precise enough to differentiate small anatomical units in sensorimotor areas. In our parcellation analysis, boundaries were only detected between upper, middle and lower limb, which was confirmed by the dominant activation area of foot, hand and tongue. These three sections might also be activated by movement of other body parts, e.g. arm and lips, which was beyond the scope of the current study. The segments also have smaller units such as toes and fingers, which could be detected by fMRI (Blankenburg *et al.*, 2003; Sanchez-Panchuelo *et al.*, 2012). In future studies, a higher spatial resolution could allow for a higher number of parcellations targeting smaller functional units. Also, the peak activity area for a specific body part, such as the tip of the index finger, could help in investigating resting-state subregions, rather than boundary detection from WTA analysis of task images (Meier *et al.*, 2008).

The estimation of the optimal number of clusters in the sensorimotor cortex required *a priori* knowledge and remains a methodological challenge. To date, several studies have taken the measure of cluster stability across bilateral areas (Kahnt *et al.*, 2012), sessions (Nebel *et al.*, 2012) and individuals (Schubotz *et al.*, 2010; Liu *et al.*, 2013) to select the optimal number of clusters. Cluster parameters such as silhouette have also been employed for cluster number validation (Kelly *et al.*, 2010). In the present study, the three body parts investigated limited the desired cluster number. Despite a range of cluster numbers investigated, we focused here on the three-cluster solution to match the number of activated areas.

The method that we performed was based on functional connectivity features from the BOLD signal correlation. The results represent somatotopic separation rather than the separation of cytoarchitectonically defined areas, i.e. BA 3a, BA 3b and BA 4 (Geyer *et al.*, 1999, 2000; Wig *et al.*, 2013a). Ongoing lines of research to identify BA regions in the SI through *in vivo* imaging (Geyer *et al.*, 2011) and functional connectivity analysis in the SI with ultra-high field imaging in monkey (Wang *et al.*, 2013) may also provide helpful tools for the validation of rs- fMRI-based parcellation approaches in the future.

Conclusions

We were able to identify segregated functional regions within the left MI/SI using rs-fMRI and validate its somatotopic arrangement through comparison to task-based activations with two independent datasets. The posteffect of the motor task on the resting-state parcellation map was observed. This methodology may also be applicable to clinical investigation requiring the identification of different body parts. The question remains regarding the level of detail that rs-fMRI may be able to provide for characterising functional regions. Improvements in spatial resolution will enable the investigation of unique dynamics between the MI and SI, as well as potentially further subdivisions consistent with cytoarchitectonic areas.

Acknowledgements

We acknowledge the funding and doctoral scholarship (XL) from the Max Planck Society. The HCP data were provided (in part) by the Human Connectome Project, WU–Minn Consortium (Principal Investigators: David Van Essen and Kamil Ugurbil; 1U54MH091657) funded by the 16 NIH Institutes and Centers that support the NIH Blueprint for Neuroscience Research, and by the McDonnell Center for Systems Neuroscience at Washington University. We also appreciate many insightful suggestions from the anonymous reviewers. These suggestions were helpful in improving our study. There are no competing interests of authors in the present study.

Abbreviations

BA, Brodmann area; DC, Dice coefficient; fMRI, functional magnetic resonance imaging; HCP, Human Connectome Project; MI, primary motor; MPI, Max Planck Institute; ROI, region of interest; rs-fMRI, resting-state functional magnetic resonance imaging; SI, primary somatosensory; WTA, winner-take-all.

References

Albert, N.B., Robertson, E.M. & Miall, R.C. (2009) The resting human brain and motor learning. *Curr. Biol.*, **19**, 1023–1027.

Amunts, K., Schleicher, A., Burgel, U., Mohlberg, H., Uylings, H.B. & Zilles, K. (1999) Broca's region revisited: cytoarchitecture and intersubject variability. *J. Comp. Neurol.*, **412**, 319–341.

Anwander, A., Tittgemeyer, M., von Cramon, D.Y., Friederici, A.D. & Knosche, T.R. (2007) Connectivity-based parcellation of Broca's area. *Cereb. Cortex*, **17**, 816–825.

Barnes, A., Bullmore, E.T. & Suckling, J. (2009) Endogenous human brain dynamics recover slowly following cognitive effort. *PLoS ONE*, **4**, e6626.

Beckmann, M., Johansen-Berg, H. & Rushworth, M.F. (2009) Connectivity-based parcellation of human cingulate cortex and its relation to functional specialization. *J. Neurosci.*, **29**, 1175–1190.

Blankenburg, F., Ruben, J., Meyer, R., Schwiemann, J. & Villringer, A. (2003) Evidence for a rostral-to-caudal somatotopic organization in human primary somatosensory cortex with mirror-reversal in areas 3b and 1. *Cereb. Cortex*, **13**, 987–993.

Brodmann, K. (1909) *Brodmann's Localisation in the Cerebral Cortex*. Johann Ambrosius Barth, Leipzig, Germany.

Buckner, R.L., Krienen, F.M., Castellanos, A., Diaz, J.C. & Yeo, B.T. (2011) The organization of the human cerebellum estimated by intrinsic functional connectivity. *J. Neurophysiol.*, **106**, 2322–2345.

Campbell, A.W. (1905) *Histological Studies on the Localization of Cerebral Function*. Cambridge University Press, Cambridge, MA.

Cauda, F., Giuliano, G., Federico, D., Sergio, D. & Katiuscia, S. (2011) Discovering the somatotopic organization of the motor areas of the medial wall using low-frequency BOLD fluctuations. *Hum. Brain Mapp.*, **32**, 1566–1579.

Cohen, A.L., Fair, D.A., Dosenbach, N.U., Miezin, F.M., Dierker, D., Van Essen, D.C., Schlaggar, B.L. & Petersen, S.E. (2008) Defining functional areas in individual human brains using resting functional connectivity MRI. *NeuroImage*, **41**, 45–57.

Cox, R.W. (1996) AFNI: software for analysis and visualization of functional magnetic resonance neuroimages. *Comput. Biomed. Res.*, **29**, 162–173.

Dice, L.R. (1945) Measures of the amount of ecologic association between species. *Ecology*, **26**, 297–302.

Duff, E.P., Johnston, L.A., Xiong, J., Fox, P.T., Mareels, I. & Egan, G.F. (2008) The power of spectral density analysis for mapping endogenous BOLD signal fluctuations. *Hum. Brain Mapp.*, **29**, 778–790.

Economo, C.V. (1926) *Eine neue Art Spezialzellen des Lobus cinguli und Lobus insulae*. *Z. Gesamte Neurol. Psy.,* **100**, 706–712.

Eickhoff, S.B., Stephan, K.E., Mohlberg, H., Grefkes, C., Fink, G.R., Amunts, K. & Zilles, K. (2005) A new SPM toolbox for combining probabilistic cytoarchitectonic maps and functional imaging data. *NeuroImage*, **25**, 1325–1335.

Fan, L., Wang, J., Zhang, Y., Han, W., Yu, C. & Jiang, T. (2013) Connectivity-based parcellation of the human temporal pole using diffusion tensor imaging. *Cereb. Cortex*, doi: 10.1093/cercor/bht196. [Epub ahead of print].

Feinberg, D.A., Moeller, S., Smith, S.M., Auerbach, E., Ramanna, S., Gunther, M., Glasser, M.F., Miller, K.L., Ugurbil, K. & Yacoub, E. (2010) Multiplexed echo planar imaging for sub-second whole brain FMRI and fast diffusion imaging. *PLoS ONE*, **5**, e15710.

Fischl, B. (2012) FreeSurfer. *NeuroImage*, **62**, 774–781.

Gentilucci, M. & Campione, G.C. (2011) Do postures of distal effectors affect the control of actions of other distal effectors? Evidence for a system of interactions between hand and mouth. *PLoS ONE*, **6**, e19793.
Geyer, S., Schleicher, A. & Zilles, K. (1999) Areas 3a, 3b, and 1 of human primary somatosensory cortex. *NeuroImage*, **10**, 63–83.
Geyer, S., Schormann, T., Mohlberg, H. & Zilles, K. (2000) Areas 3a, 3b, and 1 of human primary somatosensory cortex. Part 2. Spatial normalization to standard anatomical space. *NeuroImage*, **11**, 684–696.
Geyer, S., Weiss, M., Reimann, K., Lohmann, G. & Turner, R. (2011) Microstructural parcellation of the human cerebral cortex - from Brodmann's post-mortem map to *in vivo* mapping with high-field magnetic resonance imaging. *Front. Hum. Neurosci.*, **5**, 19.
Glasser, M.F., Sotiropoulos, S.N., Wilson, J.A., Coalson, T.S., Fischl, B., Andersson, J.L., Xu, J., Jbabdi, S., Webster, M., Polimeni, J.R., Van Essen, D.C. & Jenkinson, M. (2013) The minimal preprocessing pipelines for the Human Connectome Project. *NeuroImage*, **80**, 105–124.
Gorbach, N.S., Schutte, C., Melzer, C., Goldau, M., Sujazow, O., Jitsev, J., Douglas, T. & Tittgemeyer, M. (2011) Hierarchical information-based clustering for connectivity-based cortex parcellation. *Front. Neuroinform.*, **5**, 18.
Goulas, A., Uylings, H.B. & Stiers, P. (2012) Unravelling the intrinsic functional organization of the human lateral frontal cortex: a parcellation scheme based on resting state fMRI. *J. Neurosci.*, **32**, 10238–10252.
Heeger, D.J. & Ress, D. (2002) What does fMRI tell us about neuronal activity? *Nat. Rev. Neurosci.*, **3**, 142–151.
van den Heuvel, M.P. & Hulshoff Pol, H.E. (2010) Specific somatotopic organization of functional connections of the primary motor network during resting state. *Hum. Brain Mapp.*, **31**, 631–644.
Jenkinson, M., Bannister, P., Brady, M. & Smith, S. (2002) Improved optimization for the robust and accurate linear registration and motion correction of brain images. *NeuroImage*, **17**, 825–841.
Jenkinson, M., Beckmann, C.F., Behrens, T.E., Woolrich, M.W. & Smith, S.M. (2012) FSL. *NeuroImage*, **62**, 782–790.
Jo, H.J., Saad, Z.S., Gotts, S.J., Martin, A. & Cox, R.W. (2012) Quantifying agreement between anatomical and functional interhemispheric correspondences in the resting brain. *PLoS ONE*, **7**, e48847.
Johansen-Berg, H., Behrens, T.E., Robson, M.D., Drobnjak, I., Rushworth, M.F., Brady, J.M., Smith, S.M., Higham, D.J. & Matthews, P.M. (2004) Changes in connectivity profiles define functionally distinct regions in human medial frontal cortex. *Proc. Natl. Acad. Sci. USA*, **101**, 13335–13340.
Kaas, J.H., Nelson, R.J., Sur, M., Lin, C.S. & Merzenich, M.M. (1979) Multiple representations of the body within the primary somatosensory cortex of primates. *Science*, **204**, 521–523.
Kahnt, T., Chang, L.J., Park, S.Q., Heinzle, J. & Haynes, J.D. (2012) Connectivity-based parcellation of the human orbitofrontal cortex. *J. Neurosci.*, **32**, 6240–6250.
Kelly, C., Uddin, L.Q., Shehzad, Z., Margulies, D.S., Castellanos, F.X., Milham, M.P. & Petrides, M. (2010) Broca's region: linking human brain functional connectivity data and non-human primate tracing anatomy studies. *Eur. J. Neurosci.*, **32**, 383–398.
Kim, J.H., Lee, J.M., Jo, H.J., Kim, S.H., Lee, J.H., Kim, S.T., Seo, S.W., Cox, R.W., Na, D.L., Kim, S.I. & Saad, Z.S. (2010) Defining functional SMA and pre-SMA subregions in human MFC using resting state fMRI: functional connectivity-based parcellation method. *NeuroImage*, **49**, 2375–2386.
Knosche, T.R. & Tittgemeyer, M. (2011) The role of long-range connectivity for the characterization of the functional-anatomical organization of the cortex. *Front. Syst. Neurosci.*, **5**, 58.
Liu, H., Qin, W., Li, W., Fan, L., Wang, J., Jiang, T. & Yu, C. (2013) Connectivity-based parcellation of the human frontal pole with diffusion tensor imaging. *J. Neurosci.*, **33**, 6782–6790.
Lotze, M., Erb, M., Flor, H., Huelsmann, E., Godde, B. & Grodd, W. (2000) fMRI evaluation of somatotopic representation in human primary motor cortex. *NeuroImage*, **11**, 473–481.
Margulies, D.S., Kelly, A.M., Uddin, L.Q., Biswal, B.B., Castellanos, F.X. & Milham, M.P. (2007) Mapping the functional connectivity of anterior cingulate cortex. *NeuroImage*, **37**, 579–588.
Margulies, D.S., Vincent, J.L., Kelly, C., Lohmann, G., Uddin, L.Q., Biswal, B.B., Villringer, A., Castellanos, F.X., Milham, M.P. & Petrides, M. (2009) Precuneus shares intrinsic functional architecture in humans and monkeys. *Proc. Natl. Acad. Sci. USA*, **106**, 20069–20074.
Meier, J.D., Aflalo, T.N., Kastner, S. & Graziano, M.S. (2008) Complex organization of human primary motor cortex: a high-resolution fMRI study. *J. Neurophysiol.*, **100**, 1800–1812.
Meila, M. & Shi, J. (2001) *A Random Walks View of Spectral Segmentation. AI and Statistics (AISTATS).* Key West, Florida, January 4-7, 2001. Available http://www.gatsby.ucl.ac.uk/aistats/aistats2001/papers.html.
Moeller, S., Yacoub, E., Olman, C.A., Auerbach, E., Strupp, J., Harel, N. & Ugurbil, K. (2010) Multiband multislice GE-EPI at 7 tesla, with 16-fold acceleration using partial parallel imaging with application to high spatial and temporal whole-brain fMRI. *Magn. Reson. Med.*, **63**, 1144–1153.
Nebel, M.B., Joel, S.E., Muschelli, J., Barber, A.D., Caffo, B.S., Pekar, J.J. & Mostofsky, S.H. (2012) Disruption of functional organization within the primary motor cortex in children with autism. *Hum. Brain Mapp.*, doi: 10.1002/hbm.22188. [Epub ahead of print].
Nelson, S.M., Cohen, A.L., Power, J.D., Wig, G.S., Miezin, F.M., Wheeler, M.E., Velanova, K., Donaldson, D.I., Phillips, J.S., Schlaggar, B.L. & Petersen, S.E. (2010) A parcellation scheme for human left lateral parietal cortex. *Neuron*, **67**, 156–170.
Okada, Y.C., Tanenbaum, R., Williamson, S.J. & Kaufman, L. (1984) Somatotopic organization of the human somatosensory cortex revealed by neuromagnetic measurements. *Exp. Brain Res.*, **56**, 197–205.
Penfield, W.B. & Boldrey, E. (1937) Somatic motor and sensory representation in the cerebral cortex of man as studied by electrical stimulation. *Brain*, **60**, 389–443.
Rao, S.M., Binder, J.R., Hammeke, T.A., Bandettini, P.A., Bobholz, J.A., Frost, J.A., Myklebust, B.M., Jacobson, R.D. & Hyde, J.S. (1995) Somatotopic mapping of the human primary motor cortex with functional magnetic resonance imaging. *Neurology*, **45**, 919–924.
de Reus, M.A. & van den Heuvel, M.P. (2013) The parcellation-based connectome: limitations and extensions. *NeuroImage*, doi: 10.1016/j.neuroimage.2013.03.053. [Epub ahead of print].
Roca, P., Tucholka, A., Riviere, D., Guevara, P., Poupon, C. & Mangin, J.F. (2010) Inter-subject connectivity-based parcellation of a patch of cerebral cortex. *Med. Image. Comput. Comput. Assist. Interv.*, **13**, 347–354.
Ruschel, M., Knosche, T.R., Friederici, A.D., Turner, R., Geyer, S. & Anwander, A. (2013) Connectivity architecture and subdivision of the human inferior parietal cortex revealed by diffusion MRI. *Cereb. Cortex*, doi: 10.1093/cercor/bht098. [Epub ahead of print].
Sanchez-Panchuelo, R.M., Besle, J., Beckett, A., Bowtell, R., Schluppeck, D. & Francis, S. (2012) Within-digit functional parcellation of Brodmann areas of the human primary somatosensory cortex using functional magnetic resonance imaging at 7 tesla. *J. Neurosci.*, **32**, 15815–15822.
Sanides, F. (1970) Functional architecture of motor and sensory cortices in primates in the light of a new concept of neocortex evolution. In Noback, C.R. & Montagna, W. (Eds), *The primate brain*. Appleton-Century-Crofts, New York, pp. 137–208.
Schubotz, R.I., Anwander, A., Knosche, T.R., von Cramon, D.Y. & Tittgemeyer, M. (2010) Anatomical and functional parcellation of the human lateral premotor cortex. *NeuroImage*, **50**, 396–408.
Serra, L., Cercignani, M., Carlesimo, G.A., Fadda, L., Tini, N., Giulietti, G., Caltagirone, C. & Bozzali, M. (2013) Connectivity-based parcellation of the thalamus explains specific cognitive and behavioural symptoms in patients with bilateral thalamic infarct. *PLoS ONE*, **8**, e64578.
Setsompop, K., Gagoski, B.A., Polimeni, J.R., Witzel, T., Wedeen, V.J. & Wald, L.L. (2012) Blipped-controlled aliasing in parallel imaging for simultaneous multislice echo planar imaging with reduced g-factor penalty. *Magn. Reson. Med.*, **67**, 1210–1224.
Stippich, C., Hofmann, R., Kapfer, D., Hempel, E., Heiland, S., Jansen, O. & Sartor, K. (1999) Somatotopic mapping of the human primary somatosensory cortex by fully automated tactile stimulation using functional magnetic resonance imaging. *Neurosci. Lett.*, **277**, 25–28.
Stippich, C., Ochmann, H. & Sartor, K. (2002) Somatotopic mapping of the human primary sensorimotor cortex during motor imagery and motor execution by functional magnetic resonance imaging. *Neurosci. Lett.*, **331**, 50–54.
Swinnen, S.P. & Carson, R.G. (2002) The control and learning of patterns of interlimb coordination: past and present issues in normal and disordered control. *Acta Psychol.*, **110**, 129–137.
Taubert, M., Lohmann, G., Margulies, D.S., Villringer, A. & Ragert, P. (2011) Long-term effects of motor training on resting-state networks and underlying brain structure. *NeuroImage*, **57**, 1492–1498.
Triarhou, L.C. (2007) The Economo-Koskinas atlas revisited: cytoarchitectonics and functional context. *Stereot. Funct. Neuros.*, **85**, 195–203.
Tung, K.C., Uh, J., Mao, D., Xu, F., Xiao, G. & Lu, H. (2013) Alterations in resting functional connectivity due to recent motor task. *NeuroImage*, **78**, 316–324.

Van Essen, D.C. & Glasser, M.F. (2013) *In vivo* architectonics: a cortico-centric perspective. *NeuroImage*, doi: 10.1016/j.neuroimage.2013.04.095. [Epub ahead of print].

Van Essen, D.C., Smith, S.M., Barch, D.M., Behrens, T.E., Yacoub, E. & Ugurbil, K. (2013) The WU-Minn Human Connectome Project: an overview. *NeuroImage*, **80**, 62–79.

Vincent, J.L., Patel, G.H., Fox, M.D., Snyder, A.Z., Baker, J.T., Van Essen, D.C., Zempel, J.M., Snyder, L.H., Corbetta, M. & Raichle, M.E. (2007) Intrinsic functional architecture in the anaesthetized monkey brain. *Nature*, **447**, 83–86.

Vogt, C. & Vogt, O (1919) Ergebnisse unserer hirnforschung. *J. Psychol. Neurol.*, **25**, 279–461.

Wang, Z., Chen, L.M., Negyessy, L., Friedman, R.M., Mishra, A., Gore, J.C. & Roe, A.W. (2013) The relationship of anatomical and functional connectivity to resting-state connectivity in primate somatosensory cortex. *Neuron*, **78**, 1116–1126.

Weiss, C., Nettekoven, C., Rehme, A.K., Neuschmelting, V., Eisenbeis, A., Goldbrunner, R. & Grefkes, C. (2012) Mapping the hand, foot and face representations in the primary motor cortex – retest reliability of neuronavigated TMS versus functional MRI. *NeuroImage*, **66C**, 531–542.

Wig, G.S., Laumann, T.O., Cohen, A.L., Power, J.D., Nelson, S.M., Glasser, M.F., Miezin, F.M., Snyder, A.Z., Schlaggar, B.L. & Petersen, S.E. (2013a) Parcellating an individual subject's cortical and subcortical brain structures using snowball sampling of resting-state correlations. *Cereb. Cortex*, doi: 10.1093/cercor/bht056. [Epub ahead of print].

Wig, G.S., Laumann, T.O. & Petersen, S.E. (2013b) An approach for parcellating human cortical areas using resting-state correlations. *NeuroImage*, doi: 10.1016/j.neuroimage.2013.07.035. [Epub ahead of print].

Woolrich, M.W., Ripley, B.D., Brady, M. & Smith, S.M. (2001) Temporal autocorrelation in univariate linear modeling of FMRI data. *NeuroImage*, **14**, 1370–1386.

Xu, J.M.S., Strupp, J., Auerbach, E., Feinberg, D.A., Ugurbil, K. & Yacoub, E. (2012) Highly Accelerated whole brain imaging using aligned-blipped-controlled-aliasing multiband EPI. Vol. 20, ISMRM 20th Annual Meeting. ISMRM.

Yeo, B.T., Krienen, F.M., Sepulcre, J., Sabuncu, M.R., Lashkari, D., Hollinshead, M., Roffman, J.L., Smoller, J.W., Zollei, L., Polimeni, J.R., Fischl, B., Liu, H. & Buckner, R.L. (2011) The organization of the human cerebral cortex estimated by intrinsic functional connectivity. *J. Neurophysiol.*, **106**, 1125–1165.

Yu, C., Zhou, Y., Liu, Y., Jiang, T., Dong, H., Zhang, Y. & Walter, M. (2011) Functional segregation of the human cingulate cortex is confirmed by functional connectivity based neuroanatomical parcellation. *NeuroImage*, **54**, 2571–2581.

Zhang, S. & Li, C.S. (2012) Functional connectivity mapping of the human precuneus by resting state fMRI. *NeuroImage*, **59**, 3548–3562.